Remote Sensing of Ice Cloud Properties With Millimeter and Submillimeter-Wave Polarimetry

(article starts on next page)

Remote Sensing of Ice Cloud Properties With Millimeter and Submillimeter-Wave Polarimetry

DONG L. WU [1], JIE GONG [1] (Member, IEEE), WILLIAM R. DEAL [2] (Fellow, IEEE),
WILLIAN GAINES[3] (Member, IEEE), CAITLYN M. COOKE [2] (Member, IEEE), GIOVANNI DE AMICI[4],
PETER PANTINA[5], YULI LIU[6], PING YANG [7], PATRICK ERIKSSON [8], AND RALF BENNARTZ [9]

(Invited Paper)

[1]NASA Goddard Space Flight Center, Climate and Radiation Laboratory, Greenbelt, MD 20771 USA
[2]RF and Mixed Signal Department, Northrop Grumman Corporation, Redondo Beach, CA 90278 USA
[3]Space Remote Sensing Hardware Engineering Department, Northrop Grumman Corporation, Azusa, CA 91702 USA
[4]NASA Goddard Space Flight Center, Microwave Instrument Technology Branch, Greenbelt, MD 20771 USA
[5]Science Systems and Application Inc., Lanham, MD 20706 USA
[6]Department of Physics, University of Maryland Baltimore County, Baltimore, MD 21250 USA
[7]Department of Atmospheric Sciences, Texas A&M University, College Station, TX 77843 USA
[8]Department of Space, Earth and Environment, Chalmers University of Technology, 412 96 Gothenburg, Sweden
[9]Department of Earth and Environmental Sciences, Vanderbilt University, Nashville, TN 37235 USA

CORRESPONDING AUTHOR: Dong L. Wu (e-mail: dong.l.wu@nasa.gov).

ABSTRACT Ice clouds are poorly constrained in current global climate and weather models and have been used as a tuning parameter in the models to balance radiation budget at the top of atmosphere and precipitation at the surface. Sub-millimeter-wave (Submm) remote sensing can fill the sensitivity gap of cloud ice observations between visible/infrared (VIS/IR) and microwave (MW) frequencies. The added value from submm-wave bands has been recognized for achieving a better understanding of cloud, convection and precipitation (CCP) processes. Recent satellite observations at microwave frequencies showed promising results that additional information on cloud microphysical properties (e.g., ice particle shape and orientation) can be inferred from V-pol and H-pol radiances. Motivated by the added value from cloud polarimeters, a compact SWIRP (Submm-Wave and Long-Wave InfraRed Polarimeter) was developed under NASA's Instrument Incubator Program (IIP) to reduce instrument size, weight, power (SWaP) for future Earth science missions. Low-SWaP sensors like SWIRP will allow the cost-effective implementation of a distributed observing system to study fast cloud processes with the needed spatiotemporal sampling.

INDEX TERMS Submm-wave, MMIC, remote sensing, ice cloud, microphysics, SmallSat, microwaves in climate change.

I. INTRODUCTION

Earth climate change depends critically on how clouds react to the surface warming and interact with atmospheric radiation, dynamics, latent heating, and precipitation processes. Accurate representation of clouds in global circulation models (GCMs) is still a great challenge, because their microphysical-scale formation, development and dissipation processes are associated with large spatiotemporal variability and complex interactions with environments. Model uncertainty for climate prediction remains quite large and clouds have been a major source of this uncertainty [1]. Ice clouds, in particular, have been used as a tuning parameter in the GCMs to achieve the needed radiation balance at the top of atmosphere (TOA) and the realistic precipitation at the surface. As a result, a wide spread of modeled cloud ice values was reported [2], [3], [4]. Thus, a better observational constraint on global cloud ice is needed and highlighted in the U.S. National Academy of Sciences (NRC) *Earth Science Decadal Survey* (DS) [5].

Remote sensing of cloud ice from space has been limited by several factors. First, as shown in Fig. 1, ice water path
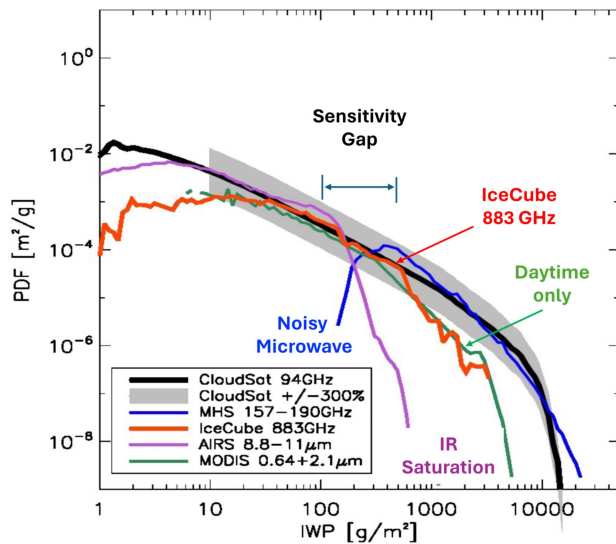
This article has been accepted for inclusion in a future issue of this journal. Content is final as presented, with the exception of pagination.

WU ET AL.: REMOTE SENSING OF ICE CLOUD PROPERTIES WITH MILLIMETER AND SUBMILLIMETER-WAVE POLARIMETRY

FIGURE 1. Cloud IWP retrieved from different satellite sensors. Sensitivity of passive IR (8–12 μm) is limited to IWP = 10–40 g/m² while the 190 GHz microwave is 200–2000 g/m². There is a gap between IR and microwave sensitivities, mostly for the upper tropospheric cloud ice where submm-wave sensors are particularly useful, as demonstrated by the IceCube mission [43], [44].

(IWP), a key parameter to characterize ice cloud mass, can vary by more than four orders of magnitude. As a result, no single sensors can cover the entire dynamic range of IWP. Second, 3-dimensional (3D) cloud structures require adequate penetration from sensors to observe cloud ice volume below the top. Compared to active remote sensing, passive sensors suffer more from the inability of capturing the full column of cloud ice. Third, cloud ice crystals consist of various shapes or habits, making the remote sensing of ice clouds even more challenging than water clouds. These microphysical properties are critical to link the measured radiances to cloud physical parameters such as IWP and effective diameter (D_{eff}), the latter of which is dependent on the particle size distribution (PSD). A large portion of the measurement uncertainty is due to different PSD assumptions used in the retrieval algorithms [6], [7].

Submm-wave remote sensing has advantage of measuring upper-tropospheric cloud ice by providing several partial columns from different frequency channels. By interacting with ice particle scattering deep inside clouds, the submm-wave sensors have a much deeper depth into the clouds than passive visible/infrared (VIS/IR) and microwave techniques [Fig. 2]. This property help fill the sensitivity gaps in cloud ice measurements. As shown in Fig. 2, the VIS/IR measurements are limited to the top 1–2 km cloud layer, not able to penetrate deep enough into ice clouds for volumetric mass measurements. Thus, these techniques rely on multiple scattering signals to infer deeper cloud properties, which lose sensitivity to microphysical properties. On the other hand, passive microwave sensors at frequencies <200 GHz are mostly sensitive to surface emission [8], liquid cloud and
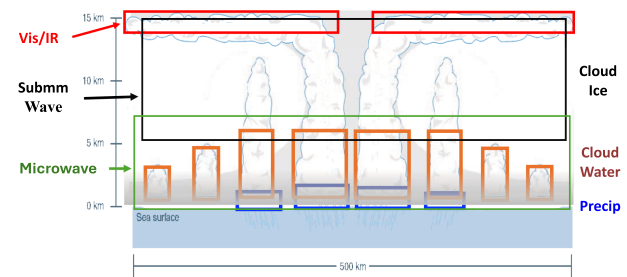

FIGURE 2. Limitations in current satellite cloud observations, showing that the VIS/IR penetration is confined mainly at the topmost layer while the low-frequency microwave is sensitive primarily to emissions from the surface and the lower atmospheric water cloud and rain.

rain [8], [10] and scattering from large precipitating frozen hydrometeors (e.g., graupel, snow) [11], [12], [13], [14].

Polarimetric measurements can add a further constraint on ice microphysical properties such as crystal shape and orientation. Very little is known about the global distribution and life cycle of these cloud ice properties. Lidar observations showed that a significant depolarization ratio exists globally due to scattering from horizontally oriented plate crystals at temperatures between −10 °C and −30 °C [15]. From passive satellite imaging measurements of the Moderate Resolution Imaging Spectroradiometer (MODIS) and Polarization and Directionality of the Earth's Reflectance (POLDER) instruments, a simultaneous retrieval of cloud optical thickness, ice effective radius, aspect ratio (AR) of ice crystals was demonstrated [16]. Atmospheric wind shears and in-cloud dynamics were found to play an important role in driving the variability of these cloud parameters. Analyzing polarized brightness temperature (TB) measurements from the Tropical Rainfall Measuring Mission (TRMM) Microwave Instrument (TMI), Prigent et al. [17] found a positive correlation between the 89-GHz polarization difference (PD) and scattering from large ice particles. PD is defined as difference between vertical (V-pol) and horizontal (H-pol) polarized TB, i.e., TBv-TBh (or V-H). The PD-TB study was recently extended to higher frequencies including 122 GHz [18], 166 and 664 GHz [19]. Compared to lower microwave frequencies, the PDs at these high-frequency channels have a smaller contribution from the surface and thus produce clearer cloud signals globally. Motivated by these high-frequency polarimetric results, benefits of submm-wave polarimeters has been recognized, especially for better understanding cloud feedback and variability in climate change.

In this study we provide an overview of our recent work on cloud remote sensing with microwave polarimetry, submm-wave instrument development, and future satellite missions with submm-wave ice cloud observations. The paper is organized to devote Section II for polarimetric cloud satellite observations from high-frequency microwave, Section III for progresses in modeling ice cloud scattering, and Sections IV for a submm-wave polarimeter concept developed under NASA's Instrument Incubator Program (IIP). In
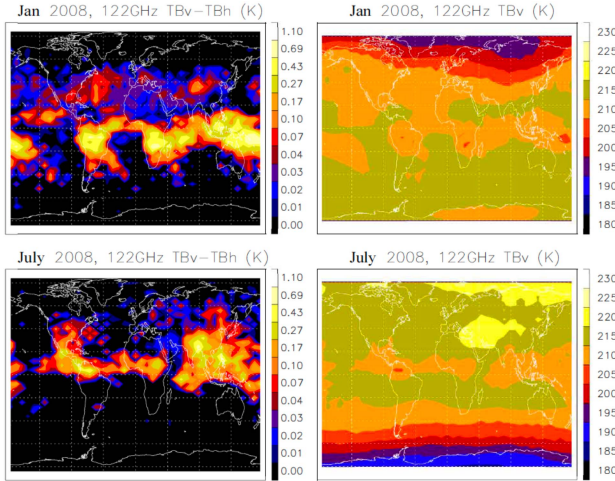
This article has been accepted for inclusion in a future issue of this journal. Content is final as presented, with the exception of pagination.

IEEE Journal of
Microwaves

FIGURE 3. Monthly all-sky average PD (V-H) and mean TB of MLS 122 GHz radiances at Ht < 5 km above the geoid for January (top) and July (bottom) 2008. A threshold of PD > 1.5 K is used for significantly polarized cloud detection and PD = 0 for the rest situations (e.g., clear sky and non-polarized clouds).

Section V, we discuss future cloud observations from the upcoming submm-wave polarimeters from ESA/EUMETSAT's Ice Cloud Imager (ICI) and NASA's Polarized Submillimeter Ice-cloud Radiometer (PolSIR).

II. POLARIZED RADIANCES FROM ICE CLOUD SCATTERING

Polarized radiances induced by ice cloud scattering are detectable by both limb and nadir viewing sensors from space. Radiative transfer model simulations suggested that only I and Q components are significant from ice particle scattering in the full Stokes (I, Q, U, V) vector from the vantage point of spaceborne sensors [7]. Thus, most of the polarization investigations have been focused on the Q component, or the PD in microwave cloud observations.

A. MLS 122 GHZ

The Microwave Limb Sounder (MLS) on NASA's Aura satellite has seven radiometers at frequencies near 118, 190, 240, and 640 GHz and 2.5 THz [20]. It has been operational since August 2004 on a sun-synchronous polar orbit. MLS can observe the radiance induced by ice cloud scattering through a window channel (away from major atmospheric emission lines) at tangent heights below ∼16 km, or the tropopause height. The 122-GHz band is a window channel near the 118-GHz O_2 emission that the MLS used for profiling temperature and pressure and had both V-pol and H-pol measurements thorough the entire mission.

Davis et al. [18] analyzed the 122-GHz radiances at tangent heights (Ht) < 5 km and found a significant PD signal associated with ice cloud scattering. Using the same algorithm as in [18], here we derived a global map of average PD and TB from the MLS 122-GHz measurements for January and July 2008 [Fig. 3]. The polarized 122-GHz radiances in Fig. 3 resembles

closely the upper-tropospheric cloud ice distributions during these months, showing high values over deep convective zones in the tropics and subtropics. Deep convections lift large ice particles to the upper troposphere, which are subsequently advected to a wider area through selective processes. The particles with horizontal orientation tend to last long in the air before they are removed by precipitation. These shaped particles with a preferred orientation are essentially responsible for the polarized MLS 122-GHz radiances from an anisotropic ice scattering of the upwelling atmospheric radiation.

Compared to nadir sounding, limb sounding is generally less attractive for cloud observations, because of highly inhomogeneous cloud structures. The line-of-sight (LOS) smearing in limb sounding make it difficult to resolve horizonal cloud distributions at scales < 100 km. However, the limb sounding could provide a better constraint on cloud top (e.g., visible sensors) or uppermost cloud ice (e.g., MLS). In all complex 3D cloud ice variations, horizontal and temporal resolutions are more desirable for model improvements because the cloud observations at these scales can have direct impacts on model convective, transport and cloud microphysical schemes.

B. GMI 89 AND 166 GHZ

Nadir and slant-view scanning polarimeters can provide process-level information on ice cloud formation and evolution. Non-spherical frozen particles and their orientation preference may evolve spatiotemporally with the thermodynamic environment and wind shear. In addition, information on ice particle habits (e.g., rosette, column, plate) from the PD observations may also help to constrain modeled cloud radiative effect, particle fall speed, and surface precipitation. Like the IWP measurements, the PD measurements from nadir and slant-view imagers represent a bulk property of ice clouds in an extended height range. Studying the V-pol and H-pol radiance measurements from the Global Precipitation Measurement (GPM) Microwave Imager (GMI) 89 and 166 GHz channels, Gong and Wu [19] mapped out not only the global distribution of these PDs but also a number of extreme weather events such as squall-line storms and hurricanes.

The GMI is a conical-scan (52.8° incident angle) radiometer with useful swath of 850 km [21]. Both 89 and 166 GHz bands are dual-pol (V and H) channels with the same-size FOV of 4.4 × 7.2 km. The instrument has been operational in space since 2014.

Fig. 4 showcases a snapshot of Hurricane Dorian as observed by GMI on September 4, 2019, during its decaying phase after it stalled north of Grand Bahama. The deadly and destructive cyclone reached the peak as a Cat-5 hurricane on September 1 at landfall in the Bahamas. Substantial damages and economic losses were reported as Dorian cruised along the coasts in the Southeastern United States and Atlantic Canada.

The Hurricane Dorian was captured by GMI on Sep 4 during its decaying stage. Compared to pre-storm time (Sep 2) [Fig. 4(g)–(h)], there were many larger cloud-induced PDs

This article has been accepted for inclusion in a future issue of this journal. Content is final as presented, with the exception of pagination.

WU ET AL.: REMOTE SENSING OF ICE CLOUD PROPERTIES WITH MILLIMETER AND SUBMILLIMETER-WAVE POLARIMETRY
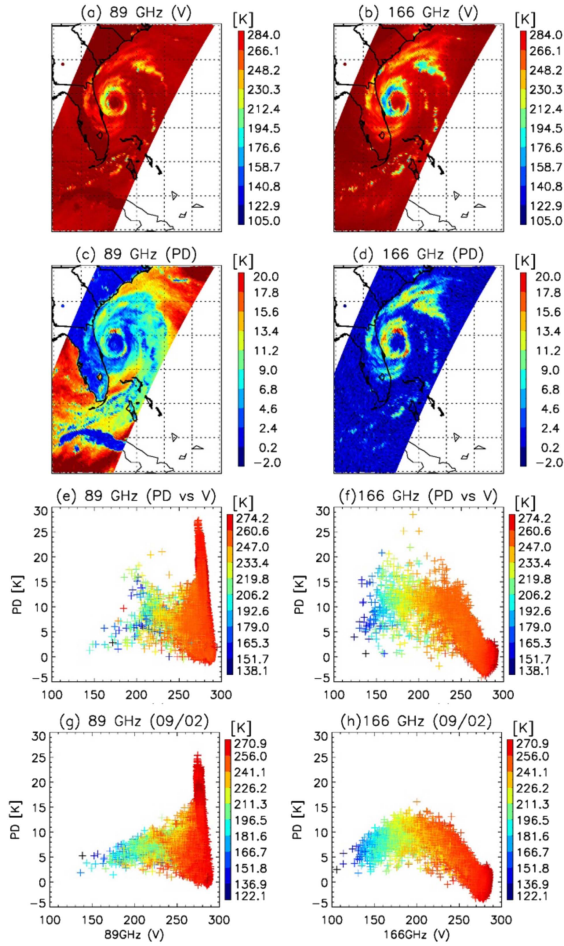
FIGURE 4. GMI 89 and 166-GHz PD (V-H) and TB maps from Hurricane Dorian on September 4, 2019, just off the East Coast of United States. In panels (e) and (f) the PD-TB scatter plots are colored by the collocated TB measurements from the GMI 183/3 GHz channel, as an indicator of cloud-top temperature. Panels (g) and (h) are same with (e) and (f), but for September 2, 2019, snapshot before the eyewall replacement.

FIGURE 5. A simplified two-layer model for the polarized radiation in cloudy-sky radiative transfer.

PD signature. Before the ERC, GMI also captured a snapshot, and the PD-TB relationships shown in Fig. 4(g) and (h) do not exhibit large PD signals. Compared to the squall-line storm studied in [19], the PD distribution from tropical storms is highly structured, correlated with the hurricane development, and hence requires a higher spatiotemporal sampling to study.

Nevertheless, useful statistical analysis can be made globally from these snapshots of deep convective systems. As shown in the previous study [19], the PD-TB relationship from the GMI 166-GHz radiance measurement is characterized by the so-called "bell-curve" [Fig. 4(e)–(h)]. Most of the cloud-induced PD show a peak at a TB between 150 K and 250 K. The PD reduces significantly in the very cold (TB < 150 K) cases where deep convective clouds reach a higher altitude. As seen in Fig. 4, the "bell-curve" relationship is valid for both extreme (e.g., hurricane) and normal weather cases. It raises an interesting question: where in clouds do these PDs come from?

By correlating the GMI 166-GHz PD with the collocated CloudSat W-band (94 GHz), GPM Ku (14 GHz) and Ka-band (35 GHz) radar profiles, Gong et al. [22] found that the cloud PDs have a clear association with the vertical distribution of frozen hydrometeors. Depending on where the PD and TB values reside in the "bell-curve" diagram, cloud-induced 166-GHz PDs are sensitive to large-size hydrometeor scattering, which becomes measurable by the Ka radar. The correlation with the W-band reflectivity suggests that the PD regimes are sensitive to the vertical distribution of ice particles. The reflectivity intensity appeared to match the PD intensity reasonably well if the reflectivity were averaged between 5–8 km.

III. MODELLING ICE CLOUDS
A. SIMPLIFIED 2-LAYER MODEL
A simplified radiative transfer model is used to comprehend some of the observed radiance features from ice cloud scattering. In this conceptual model we assume that all frozen particles are horizontally aligned with different volume scattering optical depths from V- and H-pol (τ_V and τ_H) as shown in Fig. 5. Here the AR is defined by the ratio of H/V-pol optical depths, namely, $AR \equiv \tau_H/\tau_V$. The cloud layer temperature is T_2 and the radiances at the top of atmosphere (TOA) can be expressed in a simple form

$$TB_V = T_{1V}e^{-\tau_V} + T_J\left(1 - e^{-\tau_V}\right) \qquad (1)$$

on Sep 4 [Fig. 4(e)–(f)], which reached as high as 20 K and 30 K at 89 and 166 GHz, respectively. Compared to 166 GHz, the 89-GHz channel is more sensitive to polarized water emissions from oceans (e.g., winds, salinity), while the land surface emissions are generally less polarized at these frequencies. In the satellite observations, the cloud-induced PDs are superimposed on the background emissions from the surface, creating a complex hurricane pattern in the 89-GHz PD map [Fig. 4(c)] but a much cleaner pattern in the 166-GHz PD [Fig. 4(d)].

As suggested in a squall line study [19], these large PDs are likely associated with the preference of horizontally oriented large frozen aggregates. Note that they are confined mostly around the eyewall, as Dorian underwent an eyewall replacement cycle (ERC) and weakened to Cat 2. The 89-GHz eyewall exhibits a slightly smaller eyewall diameter than the 166-GHz. During September 2–5, While the cyclone prepared to head the north, its leading arm in the upper troposphere was associated with a large amount of cloud ice and a strong
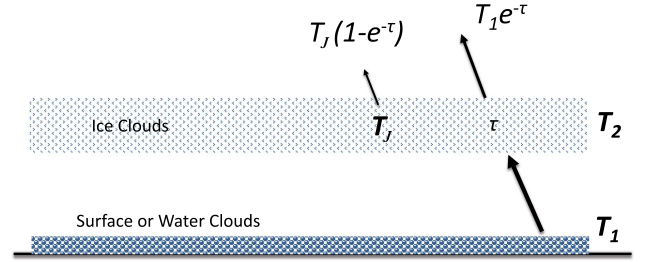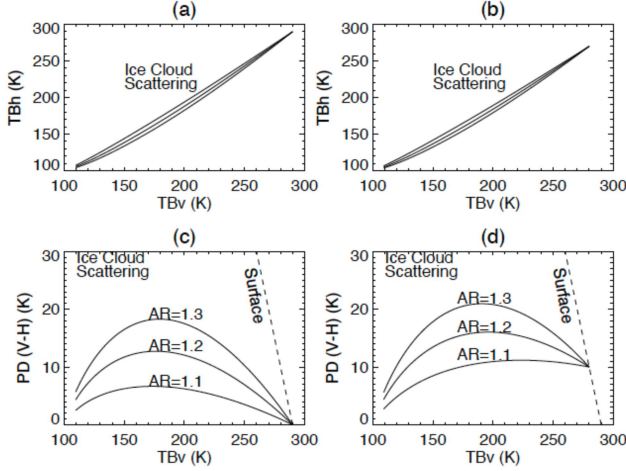
FIGURE 6. The PD -TB relationships derived from the simple model (1)–(2) that is generally applicable to all sounder frequency pairs. For a pair of polarized channels, the radiances are determined by different cloud τ_V and τ_H, and AR ($\equiv \tau_H/\tau_V$). Simulations from cloud ARs (1.1, 1.2, and 1.3) for an unpolarized ($T_{1V} - T_{1H} = 0$) and polarized ($T_{1V} - T_{1H} = 10$K) surface emissions are shown in the left (a), (c) and right (b), (d) panels. T_1 and T_J are set to be 290 K and 100 K respectively in this calculation.

$$TB_H = T_{1H}e^{-\tau_H} + T_J\left(1 - e^{-\tau_H}\right) \qquad (2)$$

where $T_{1V} = \varepsilon_V T_1$ and $T_{1H} = \varepsilon_H T_1$ are the polarized background radiances from the surface or water cloud emissions at temperature T_1. T_J is the source function of ice clouds that is a combination of scattering (T_{scat}) and upwelling emission, i.e., $(1 - \omega_0)T_1 + \omega_0 T_{scat}$, where ω_0 is the cloud single scattering albedo. T_J is a function of T_2, τ_V and τ_H, and cloud temperature T_2 is assumed a constant in the simplified model.

The conceptual model (1)–(2) can capture most of the fundamental features as observed by MLS and GMI [Fig. 6]. It predicts the "bell curve" in the observed PD-TB relationship and the "bell curve" can have different amplitudes as a function of AR. The higher the AR, the larger the PD amplitudes [Fig. 6(c)]. In the case where the surface emission is polarized, such as those from the GMI 89-GHz channel, the PD can start from a non-zero point because of the combined effect of polarized surface emission and cloud scattering.

The simplified 2-layer model can predict a reduced PD at very large τ_V and τ_H from the saturation effect. Even when the AR remains same, the PD sensitivity to AR is significantly reduced in the case of large cloud τ where the attenuation by clouds is so strong that the radiances from both channels essentially measure the similar temperature of cloud top layer. In other words, the "bell-curve" in the PD-TB relation resembles the situation where the frequencies of two sounding channels are very close to each other such as the 11 and 12 μm band in IR imagery [23]. For ice clouds, the high τ cases are often associated with irregular large crystal shapes in a strong turbulent dynamic environment. The diminishing PD due to the saturation effect makes it difficult to infer the microphysical property related to particle orientation in the high τ cases. This problem can be mitigated to some extent by selecting submm-wave frequencies (e.g., 220 GHz vs 680 GHz) that have
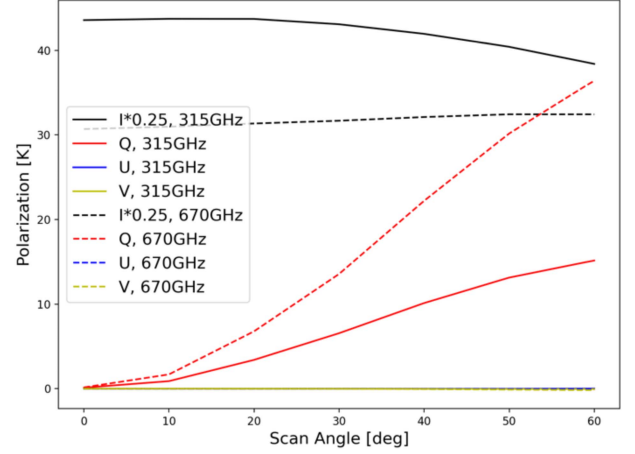

FIGURE 7. The ARTS simulations of cloud-sky ice cloud scattering as a function of the scan angle from nadir. The V-pol and H-pol are defined as the vertical and horizontal to the surface plane. Full-Stokes (I, Q, U, V) components of the 315 and 670 GHz radiances are shown to illustrate their relative importance with respect to view angle.

different sensitivities to cloud ice scattering. The simplified model was found particularly useful for all-sky radiance data assimilation of high-frequency polarized microwave radiances [24] and reduction of cloud ice retrieval uncertainty [25].

B. FULLY-POLARIZED RTM SIMULATIONS

More sophisticated simulations of the PD-TB relation can be derived with a radiance model such as the Atmospheric Radiative Transfer Simulator (ARTS) [26], which solves a pencil beam radiative transfer equation with the full Stokes vector up to 3 THz. It is capable of handling spherical 1-D to 3-D geometry and scattering calculations with the Discrete Ordinate Iterative (DOIT) or Monte Carlo (MC) solver. The ARTS model can also calculate the Jacobians of input atmospheric state variables.

Fig. 7 shows a full-Stokes (I, Q, U, V) simulation of cloudy-sky radiances at 325 and 670 GHz from different scan angles with respect to nadir. The spherical geometry is considered in this simulation where the atmosphere is characterized with spherically homogenous layers. It has a cloud layer at 10–14 km with IWP of 0.29 kg/m^2 and snow water path (SWP) of 1.6 kg/m^2, a liquid water layer below 4 km with a rainwater path (RWP) of $\sim$0.1 kg/m^2. The modified gamma function is assumed for the ice particle PSD. For ice and snow particles, plate aggregates are used in the simulations. Most of hydrometeors are oriented horizontally with a small canting angle that are randomly distributed with a 5° standard deviation [27], [28].

Scattering for cloud asymmetric ice particles induces the radiation with partial polarization, which is dominated by the Q component and increases with the scan angle toward the limb. Unlike the polarized signals (e.g., surfaces and rain) at low-frequency microwaves [29], [30], the submm-wave U and V components from ice clouds are negligible compared to Q. This is largely because the horizontally oriented
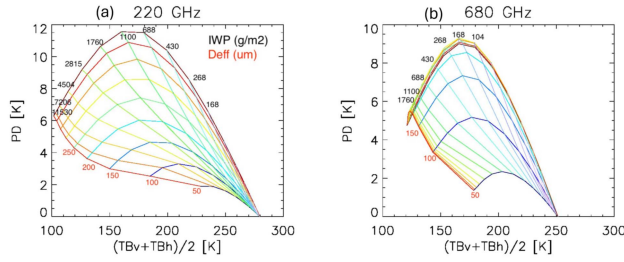
This article has been accepted for inclusion in a future issue of this journal. Content is final as presented, with the exception of pagination.

WU ET AL.: REMOTE SENSING OF ICE CLOUD PROPERTIES WITH MILLIMETER AND SUBMILLIMETER-WAVE POLARIMETRY

FIGURE 8. Simulated look-up-table (LUT) using a 100% horizontally aligned column ice crystal shape for (a) PD-TB relation at 220 GHz and (b) PD-TB relationship at 680 GHz. IWP (black) and D_{eff} (red) variations are resolved by dual-pol PD and TB measurements, greatly reducing the uncertainties in cloud ice retrievals. The simultaneous 220 and 680 GHz measurements provide the needed sensitivity to cover a large dynamic range in IWP (50-20000 g/m^2) and in D_{eff} (50-300 μm).

FIGURE 9. SWIRP spectral windows, 10 GHz near 220 GHz and 17 GHz near 680 GHz, for ice cloud measurements. Nadir-viewing spectra near 220 and 680 GHz reveal significant spectral features from atmospheric H_2O and O_3 absorption, which can vary with space and time, inducing additional uncertainty in cloud detection.

particles tend to produce little or equally important scattering polarization at $\pm 45°$ for U and little scattering circular polarization for V.

Fig. 8 summarizes a set of simulations for 220 and 680 GHz in a look-up table (LUT), in which the PD-TB curves serve as a basis for the joint retrieval of IWP and D_{eff} from a dual-band polarimeter. In these ARTS simulations the variations from IWP and D_{eff} are equivalent to the manipulation of τ_V and τ_H in (1)–(2). In addition to the LUT for the PD-TB relation, one may use the LUTs between difference frequency channels to retrieve IWP and D_{eff}, which has been demonstrated by Coy et al. [31]. Depending on the ice particle habit or a combination of habits used in these simulations, these LUTs may differ to some degree from each other. By having two frequency bands with dual polarizations, the polarimetric and radiometric information help to further constrain the IWP and D_{eff} retrievals, where ice habit or orientation can induce up to 40% uncertainty.

C. ICE PARTICLE SCATTERING MODELING

Self-consistency across different sensor wavelengths is important in radiative transfer models of ice crystal scattering and extinction coefficients. Due to computational limitations, these coefficients have been treated separately in the models for visible and microwave remote sensors. At mm- and submm-wave frequencies, Eriksson et al. [32] developed an oriented ice particle scattering database for two particle habits for 35 frequencies ranging between 1–864 GHz. This database allows users to specify a canting angle distribution with different width parameters, so to allow orientation angles from fully-random to fully-horizontally-aligned. The GPM team developed a similar database for a few other ice habits with degree of melting considered [27]. By incorporating a more sophisticated surface emissivity model, ARTS simulations can reproduce most of the observed 166-GHz PDs realistically over land and water [33]. Moreover, the PD observations can be injected now into global data assimilation systems to increase the use of polarized radiances with a reduced measurement error for these polarization channels [24].

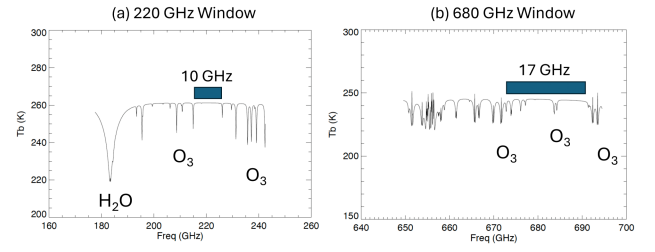A breakthrough was made recently in computation algorithm, efficiency and accuracy, such that scattering, absorption, and polarization properties of ice particles can be all calculated consistently over the spectral range from 0.2 to 100 μm [34]. This new data library (~200 GB) for the ice scattering, absorption, and polarization properties has been developed and incorporated to the ARTS model. This is a significant advance in ice cloud remote sensing since it offers an unprecedented opportunity to unify the ice cloud observations from sensors at very different wavelengths (e.g., visible, IR, and submm-wave).

IV. SWIRP INSTRUMENT

Compared to cross-track scanning instruments, conical-scanning systems have more challenges in the SWaP reduction. To meet the challenging SWaP requirement, the submm-wave and longwave IR polarimeters (SWIRP) was motivated to develop a combined compact submm-wave and IR polarimeter. SWIRP sought a low-SWaP solution for submm-wave polarimeters with an advanced 25-nm indium phosphide (InP) High Electron Mobility Transistor (HEMT) monolithic microwave integrated circuit (MMIC) receiver technology. The MMIC polarimeters use the direct detection method to make cloud measurements at 220 and 680 GHz. These low SWaP polarimeters would allow them to be packaged in a relatively small cylinder where low power is necessary for heat dissipation in space operation. The two spectral bands near 220 and 680 GHz are chosen to minimize atmospheric variations from the H_2O and O_3 attenuation for improved cloud detection [Fig. 9].

Developed under NASA's ESTO (Earth Science Technology Office) IIP program, the SWIRP's objective is to accurately measure cloud ice and its microphysical properties (particle size and shape) with combined submm-wave (220 and 680 GHz) and longwave (LW) IR (8.6, 11, and 12 μm) polarimeters. The combined submm-wave and LWIR sensitivities would cover the nearly entire dynamic range of cloud ice. The SWIRP conical scan with collocated FOVs from all frequencies helps to preserve V-pol and H-pol radiances induced by bulk cloud ice particles and their shape/orientation. The SWIRP development aimed to have a compact design so that it would have a low size, weight, power (SWaP) instrument in future cloud observations.
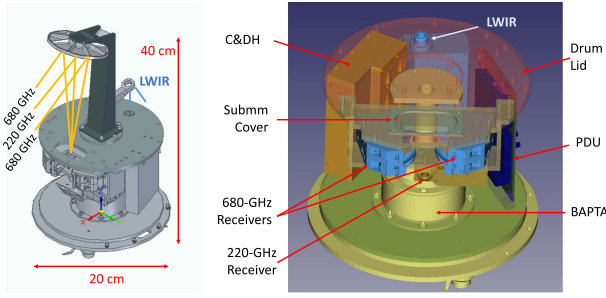
This article has been accepted for inclusion in a future issue of this journal. Content is final as presented, with the exception of pagination.

IEEE Journal of
Microwaves

FIGURE 10. SWIRP design for conical-scanning polarimeters for space operation on a 430-km orbit.
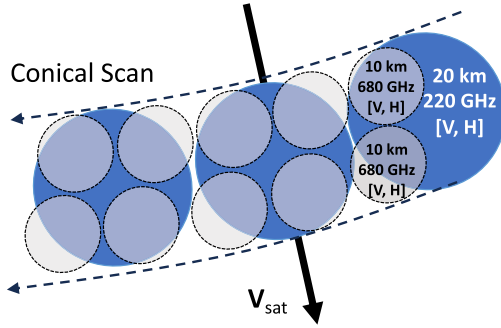

FIGURE 11. Collocated footprints of SWIRP 220 and 680 GHz polarimeters at the 41.3° incident angle. The 220-GHz footprint size is roughly twice as large as the 680-GHz one by design. With two 680-GHz polarimeters, there are no gaps in the swath of each scan. The conical scan at a constant rate of 18.7 rpm preserves the V-pol and H-pol of each measurement and continuous spatial coverage without along-track gaps from a 430 km orbit.

In this section we present an overview of the SWIRP concept and design with focus on the submm-wave instrument. Previous studies discussed the SWIRP submm-wave polarimeters [35], [37] and LWIR polarimeter [38] in great details.

A. POLARIMETER ASSEMBLY

The SWIRP instrument has a volume of 20 cm in diameter and 40 cm in height [Fig. 10]. The cylinder or drum is used to house one 220 GHz, two 680 GHz polarimeters, one LWIR polarimeter, power distribution unit (PDU), and Command and Data Handling (C&DH), which spins on a miniaturized Bearing and Power Transfer Assembly (mini-BAPTA). It scans conically at a rate of 18.7 rpm with a view angle of 38.2° from nadir, which yields 41.3° incidence angle at the surface from a 430 km orbit. The conical scans at 18.7 rpm cover the swath without significant sampling gaps with footprint sizes of 20 km at 220 GHz and 10 km at 680 GHz, respectively [Fig. 11]. The calibration targets and their electronics are the stationary subsystem (not shown here), less critical in terms of the SWaP inside the spinning drum. They are mounted on the supporting structure that occupies a roughly half of the conical FOV. All data, commands, timing and telemetry signals and power pass through the mini-BAPTA's slipring connectors to the rotating assembly [Fig. 12]. The 220 GHz polarimeter has twice long integration time (26.8 millisecond) as one for the
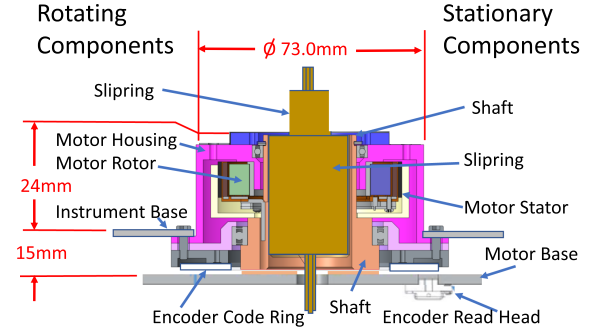

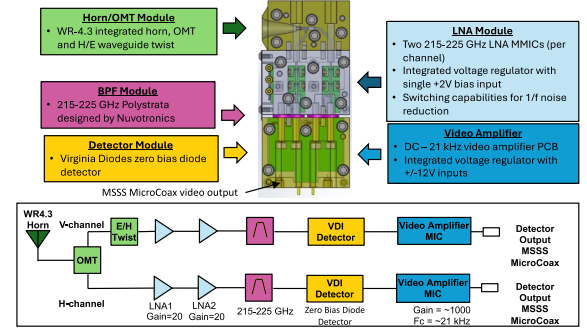**FIGURE 12.** A schematic of the SWIRP mini-BAPTA.

FIGURE 13. The SWIRP 220-GHz direct-detection polarimeter with dimensions of 1.8 × 3.0 × 6.4 cm and DC power of 0.52 W.

two 680 GHz polarimeters (13.4 millisecond) so that each 220 GHz footprint would contain four 680 GHz ones.

The SWIRP mini-BAPTA, leveraging a successful design from previous flight missions, consists of motor, drive electronics, encoder, and slipring connections [Fig. 12]. The slipring module provides 42 rings and separate connectors for power and data throughputs for each of the major subsystems. The encoder has capability of 12,000 pulses per revolution to enable system spin rate between 10–40 rpm. SWIRP chose the constant rate of 18.7 rpm for space operation. The data rate allowance is up to 400 kbps, with a comfortable margin for the SWIRP 59 kbps requirement.

B. 220 GHZ POLARIMETRIC RECEIVER

The SWIRP 220-GHz polarimeter employed the 25-nm InP HEMT low noise amplifier (LNA) technology for direct detection [35]. Compared to the heterodyne receivers, the direct detection polarimeter reduces DC power consumption by ∼10 × with a comparable noise figure of 5.1 and 5.4 dB for the H and V channels, respectively. The MMIC polarimeter has a compact dimension of 1.8 × 3.0 × 6.4 cm and employs the LNA modulation technique [36], to mitigate the 1/f noise known to the direct detection technique [Fig. 13]. The bias modulation technique is essentially a fast switching calibration against a reference in the LNA circuitry. By time sharing with the reference, it takes a $\sqrt{2}$ hit in NEdT (Noise Equivalent Temperature Difference) but helps to overcome the 1/f noise if a long integration time is needed for cloud measurements.
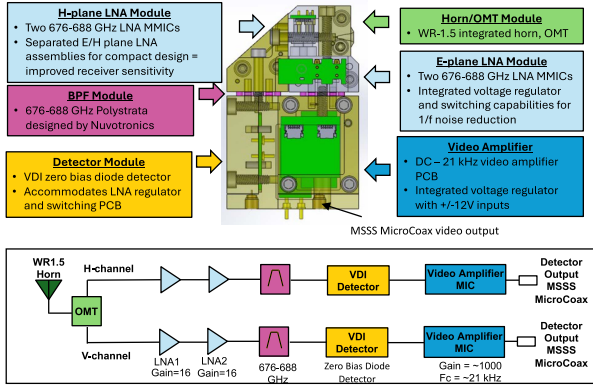
This article has been accepted for inclusion in a future issue of this journal. Content is final as presented, with the exception of pagination.

WU ET AL.: REMOTE SENSING OF ICE CLOUD PROPERTIES WITH MILLIMETER AND SUBMILLIMETER-WAVE POLARIMETRY

FIGURE 14. Block diagram of the SWIRP 680 GHz polarimetric receiver. A 1/*f* noise mitigation module is included in blue (see detailed discussions). Purple boxes are the bandpass filters built by VDI and Nuvotronics. Dimensions of 2.6 x 3.1 x 5.8 cm. DC power 1.4W.

TABLE 1. SWaP Comparisons of SWIRP With Future Satellite Missions With Submm-Wave Polarimeters

Instrument	ICI (ESA/EUMETSAT)		PolSIR (NASA EV-I)	AOS-Storm (NASA/CNES)	SWIRP (NASA/IIP)
Platform	EPS-SG		12-U CubeSat	Mid-Size Bus	SmallSat
Frequency (GHz)	183.31 ±8.4(V) 183.31 ±3.4(V) 183.31 ±2.0(V) 243.2 ±2.5 (V,H) 664 ±4.2(V,H)	325.15 ±9.5(V) 325.15 ±3.5(V) 325.15 ±1.5(V) 448 ±7.2(V) 448 ±3.0(V) 448 ±1.4(V)	325.15 ±1.5(V) 325.15 ±3.5(V) 325.15 ±9.5(V,H) 684 (V,H)	89 (1CH) 183.31 (6CH) 325.15 (3CH)	1x 220 (V,H) 2x 680 (V,H)
Mass (kg)	80		28	50	15
Scan	Conical		Cross-track	Cross-track	Conical
Size (cm)	120 X 150 X 70		35 X 20 X 20	80 X 45 X 45	40 X 20 X 20
Power (W)	80		28	55	20
Cloud Variables	AR (full swath view) IWP, D_{eff}		AR (45º view), IWP, D_{eff}	AR (45º view), IWP, D_{eff}	AR (full), IWP, D_{eff}

Prior to the SWIRP polarimeter development, other efforts were made to advance low-power MMIC detection technology at mm- and submm-wave frequencies, including the 35-nm InP HEMT receivers 89, 165, 176, 180 and 182 GHz for the Tropical Systems Technology Demonstration (TEMPEST-D) [39] and the 25-nm InP HEMT receivers at 240, 310 and 670 GHz for the Tropospheric Water and Could Ice (TWICE) [40]. These technology advances played a critical role in the SWIRP polarimeter maturation.

C. 680 GHZ POLARIMETRIC RECEIVERS

The SWIRP 680-GHz direct detection receiver demonstrated an unprecedented SWaP as a dual-pol polarimeter [37]. It leveraged the technology advancement and capabilities achieved by the TWICE project that produced high sensitivity amplifiers and a brassboard receiver with 30 GHz bandwidth. The SWIRP polarimeters further reduced the bandwidth of direct detection to 17 GHz with closely matched filter responses for both V-pol and H-pol channels.

The SWIRP 680-GHz polarimeter has a very compact, efficient architecture design. It employs a dual-pol horn, instead of two receivers with orthogonal apertures, to achieve a compact low-mass 2-elementary polarimeter array. As shown in Fig. 14, the feed horn antenna passes the submm-wave radiation from the scene to an integrated orthomode transducer (OMT). One of the OMT outputs is switched to V-pol using the E/H twist module. Followed by the LNA housings, the amplified noise power is then band-passed by a narrow-band (17 GHz) filter and detected by a zero bias detector manufactured by the Virginia Diodes Incorporated (VDI). Finally, a video amplifier (blue blocks in Fig. 14) outputs the analog voltage, ready for an analogue-to-digital converter (ADC). A voltage regulator is integrated for V-pol and H-pol separately to enable switching capabilities for 1/*f* noise reduction [37].

The OMT-E/H twist technique is commonly used for low-frequency (<200 GHz) polarization channels, but rarely at 680 GHz. The signal quality such as cross-pol for 680 GHz hence needs to be further measured and demonstrated for future spaceborne applications. Other existing submm-wave receivers (e.g., TWICE) currently uses a polarized splitter to enable both V-pol and H-pol measurements, leading to doubled power and mass for the similar polarimeter.

A novel 1/*f* noise mitigation technique has significantly improved receiver sensitivity, which was developed for the 670-GHz MMIC receivers and demonstrated by the TWICE project [36], [41]. Like the reference load in a Dicke-switched radiometer, the new technique tracks and remove 1/*f* noise fluctuations against a reference by switching on and off the first LNA MMIC transistor. The output during the transistor off-state is an independent reference, which manifests itself as 1/*f* noise fluctuations of the antenna signal in the transistor on-state. Despite the penalty of $\sqrt{2}$ in noise, the on-and-off switching for 1/*f* noise reduction is still beneficial for short-integration measurements.

V. FUTURE ICE CLOUD OBSERVATIONS

Future satellite missions have a strong demand for low-SWaP instruments to enable cost-effective cloud observations. Since clouds are highly variable in space and time with a large dynamic range and different types of water content, it requires a distributed spaceborne system to observe these fast processes. Table 1 compares the SWaP parameters and science capabilities of SWIRP with upcoming satellite missions for ice cloud observations. The missions with only single polarization channels cannot identify ice particle shape or orientation information (i.e., AR), and therefore not included in this comparison.

A. ICI

Ice Cloud Imager (ICI) is one of the five instruments to be flown on EUMETSAT's MetOp-SG-B (Second Generation-B) operational satellites with the first launch planned for 2026. Like the current MetOp operational satellites, MetOp-SG-B will likely be placed in an 830-km sun-synchronous orbit with the LTDN (Local Time at Descending Node) at 0930 hours. Together with the Microwave Imager (MWI) on MetOp-SG-B, the two conical-scan instruments will cover frequency bands from 18.7 to 664 GHz with two polarized bands (243 and 664 GHz) from ICI. The mm- and submm-wave bands from MetOp-SG-B will no doubt serve as the most

comprehensive sensor suite for studying ice clouds and their microphysical properties [42].

B. POLSIR

The Polarized Submillimeter Ice-cloud Radiometer (PolSIR) is a recently selected NASA Earth Venture Instrument (EVI) mission to better characterize and understand the diurnal variability of tropical and sub-tropical ice clouds. It consists of two 12U CubeSats, each equipped with two cross-track scanning submm-wave polarimeters at 325 and 684 GHz, flying in separate precessing orbits for a full diurnal sampling of 35°S–35°N latitudes monthly. Complementary to the Program of Record (PoR) missions, PolSIR seeks to (1) constrain the seasonally influenced diurnal cycle amplitude, form, and timing of IWP and D_{eff} in tropical and sub-tropical ice clouds; and (2) determine the diurnal variability of ice clouds in the convective outflow areas and understand relation to deep convection. PolSIR will significantly leverage the successful spaceflight demonstration of the 883-GHz cloud radiometer from the IceCube project [43], [44] and VDI's commercial polarimeter maturation at 325 and 680 GHz under the Small Business Innovation Research (SBIR) program.

C. AOS

Atmosphere Observing System (AOS) is a component of the NASA's future Earth System Observatory (EOS) to provide key information on the changing planet with strong international participations. It will make critical measurements for a better understanding of aerosol and cloud processes that drive global climate change and extreme weather. The AOS-Storm is the inclined-orbit component of the planned observing system with a microwave radiometer to measure IWP, precipitation, atmospheric temperature and humidity. Ice cloud observations will come primarily from the 183 and 325 GHz bands with a joint retrieval of atmospheric humidity and IWP.

VI. CONCLUSION

Submm-wave remote sensing has been recognized as a valuable technique to fill the sensitivity gap in cloud ice measurements from conventional VIS/IR and microwave sensors. Interesting microwave polarization observations have been reported from various satellite limb and nadir sensors at 89, 122, and 166 GHz, showing additional information on ice microphysical properties (e.g., crystal shape and orientation).

Radiative transfer models of ice cloud scattering have advanced significantly in recent years and can realistically simulate the observed PD-TB relation (e.g., the "bell-curve") as well as the full Stokes vector. At submm-wave, cloud asymmetric ice particles induce the radiation with partial polarization that is dominated by the Q component.

Future satellite missions require low-SWaP instruments for cost-effective distributed observing systems to observe fast processes like ice clouds with a sufficient spatiotemporal sampling. The SWIRP instrument development was aimed to achieve such a low-SWaP goal by infusing the new MMIC direct detection technology for a compact lower-power polarimeter. Although the SWIRP instrument development ended at a technological readiness level (TRL = 4), it still represents one of the most promising pathways for future low-SWaP mm- and submm-wave missions. As highlighted in this study, the SWIRP science capabilities for ice cloud measurements are comparable to some of the upcoming satellite missions.

REFERENCES

[1] IPCC, "Climate change 2023: Synthesis report," in *Contribution of Working Groups I, II and III to the Sixth Assessment Report of the Intergovernmental Panel on Climate Change*, H. Lee and J. Romero, Eds., Geneva, Switzerland: IPCC, 2023, p. 184, doi: 10.59327/IPCC/AR6-9789291691647.

[2] D. E. Waliser et al., "Cloud ice: A climate model challenge with signs and expectations of progress," *J. Geophys. Res., CloudSat Special Sect.*, vol. 114, 2009, Art. no. D00A21, doi: 10.1029/2008JD010015.

[3] J.-L. F. Li et al., "An observationally-based evaluation of cloud ice water in CMIP3 and CMIP5 GCMs and contemporary reanalyses using contemporary satellite data," *J. Geophys. Res.*, doi: 10.1029/2012JD017640.

[4] D. I. Duncan and P. Eriksson, "An update on global atmospheric ice estimates from satellite observations and reanalyses," *Atmos. Chem. Phys.*, vol. 18, pp. 11205–11219, 2018, doi: 10.5194/acp-18-11205-2018.

[5] National Academies of Sciences, Engineering, and Medicine, *Thriving on Our Changing Planet: A Decadal Strategy for Earth Observation From Space*. Washington, DC, USA: National Academies Press, 2018, doi: 10.17226/24938.

[6] D. L. Wu et al., "Comparisons of global cloud ice from MLS, CloudSat, and correlative data sets," *J. Geophys. Res., CloudSat Special Sect.*, vol. 114, 2009, Art. no. D00A24, doi: 10.1029/2008JD009946.

[7] P. Eriksson, B. Rydberg, and S. A. Buehler, "On cloud ice induced absorption and polarisation effects in microwave limb sounding," *Atmos. Meas. Techn.*, vol. 4, pp. 1305–1318, 2011, doi: 10.5194/amt-4-1305-2011.

[8] F. J. Wentz, "Measurement of the oceanic wind vector using satellite microwave radiometers," *IEEE Trans. Geosci. Remote Sens.*, vol. 30, no. 5, pp. 960–972, Sep. 1992.

[9] D. Atlas and C. W. Ulbrich, "Path and area integrated rainfall measurement by microwave attenuation in the 1–3 cm band," *J. Appl. Meteorol.*, vol. 16, no. 4, pp. 327–332, 1977.

[10] C. W. O'Dell, F. J. Wentz, and R. Bennartz, "Cloud liquid water path from satellite-based passive microwave observations: A new climatology over the global oceans," *J. Climate*, vol. 21, pp. 1721–1739, 2008, doi: 10.1175/2007JCLI1958.1.

[11] R. Wu and J. A. Weinman, "Microwave radiances from precipitating clouds containing aspherical ice, combined phase, and liquid hydrometeors," *J. Geophys. Res.*, vol. 89, pp. 7170–7178, 1984.

[12] F. Weng and N. C. Grody, "Retrieval of ice cloud parameters using a microwave imaging radiometer," *J. Atmos. Sci.*, vol. 57, pp. 1069–1081, 2000, doi: 10.1175/1520-0469(2000)057.

[13] R. Bennartz and P. Bauer, "Sensitivity of microwave radiances at 85–183 GHz to precipitating ice particles," *Radio Sci.*, vol. 38, 2003, Art. no. 8075, doi: 10.1029/2002RS002626.

[14] R. Y. Chen and R. Bennartz, "Sensitivity of 89-190-GHz microwave observations to ice particle scattering," *J. Appl. Meteorol. Climatol.*, vol. 59, pp. 1195–1215, 2020, doi: 10.1175/jamc-d-19-0293.1.

[15] V. Noel and H. Chepfer, "A global view of horizontally oriented crystals in ice clouds from cloud-aerosol LiDAR and infrared pathfinder satellite observation (CALIPSO)," *J. Geophys. Res.*, vol. 115, 2010, Art. no. D00H23, doi: 10.1029/2009JD012365.

This article has been accepted for inclusion in a future issue of this journal. Content is final as presented, with the exception of pagination.

WU ET AL.: REMOTE SENSING OF ICE CLOUD PROPERTIES WITH MILLIMETER AND SUBMILLIMETER-WAVE POLARIMETRY

[16] B. van Diedenhoven, A. M. Fridlind, B. Cairns, and A. S. Ackerman, "Variation of ice crystal size, shape, and asymmetry parameter in tops of tropical deep convective clouds," *J. Geo- Phys. Res. Atmos.*, vol. 119, pp. 11,809–11,825, 2014, doi: 10.1002/2014JD022385.

[17] C. Prigent, E. Defer, J. R. Pardo, C. Pearl, W. B. Rossow, and J.-P. Pinty, "Relations of polarized scattering signatures observed by the TRMM microwave instrument with electrical processes in cloud systems," *Geophys. Res. Lett.*, vol. 32, 2005, Art. no. L04810, doi: 10.1029/2004GL022225.

[18] C. P. Davis et al., "Cirrus induced polarization in 122 GHz aura microwave limb sounder radiances," *Geophys. Res. Lett.*, vol. 32, 2005, Art. no. L14806, doi: 10.1029/2005GL022681.

[19] J. Gong and D. L. Wu, "Microphysical properties of frozen particles inferred from Global Precipitation Measurement (GPM) Microwave Imager (GMI) polarimetric measurements," *Atmos. Chem. Phys.*, vol. 17, pp. 2741–2757, 2017, doi: 10.5194/acp-17-2741-2017.

[20] J. W. Waters et al., "The earth observing system microwave limb sounder (EOS MLS) on the aura satellite," *IEEE Trans. Geosci. Remote Sens.*, vol. 44, no. 5, pp. 1075–1092, May 2006.

[21] D. W. Draper, D. A. Newell, F. J. Wentz, S. Krimchansky, and G. M. Skofronick-Jackson, "The global precipitation measurement (GPM) microwave imager (GMI): Instrument overview and early on-orbit performance," *IEEE J. Sel. Top. Appl. Earth Observ. Remote Sens.*, vol. 8, no. 7, pp. 3452–3462, Jul. 2015, doi: 10.1109/JSTARS.2015.2403303.

[22] J. Gong et al., "Linkage among ice crystal microphysics, mesoscale dynamics, and cloud and precipitation structures revealed by collocated microwave radiometer and multifrequency radar observations," *Atmos. Chem. Phys.*, vol. 20, pp. 12633–12653, 2020, doi: 10.5194/acp-20-12633-2020.

[23] R. W. Saunders and K. T. Kriebel, "1988: An improved method for detecting clear sky and cloudy radiances from AVHRR data," *Int. J. Remote Sens.*, vol. 9, no. 1, pp. 123–150, 1988.

[24] V. Barlakas, A. J. Geer, and P. Eriksson, "Introducing hydrometeor orientation into all-sky microwave and submillimeter assimilation," *Atmos. Meas. Techn.*, vol. 14, pp. 3427–3447, 2021, doi: 10.5194/amt-14-3427-2021.

[25] I. Kaur et al., "Fast radiative transfer approximating ice hydrometeor orientation and its implication on IWP retrievals," *Remote Sens.*, vol. 14, 2022, Art. no. 1594, doi: 10.3390/rs14071594.

[26] S. A. Buehler et al., "A concept for a satellite mission to measure cloud ice water path, ice particle size, and cloud altitude," *Quart. J. Roy. Meteorological Soc., J. Atmos. Sci., Appl. Meteorol. Phys. Oceanogr.*, vol. 133, pp. 109–128, 2007, doi: 10.1002/qj.143.

[27] J. A. Milbrandt and M. K. Yau, "A multimoment bulk microphysics parameterization. Part I: Analysis of the role of the spectral shape parameter," *J. Atmos. Sci.*, vol. 62, pp. 3051–3064, 2005.

[28] M. Brath, R. Ekelund, P. Eriksson, O. Lemke, and S. A. Buehler, "Microwave and submillimeter wave scattering of oriented ice particles," *Atmos. Meas. Techn.*, vol. 13, pp. 2309–2333, 2020, doi: 10.5194/amt-13-2309-2020.

[29] R. W. Spencer, H. M. Goodman, and R. E. Hood, "Precipitation retrieval over land and ocean with the SSM/I: Identification and characteristics of the scattering signal," *J. Atmos. Ocean. Technol.*, vol. 6, pp. 254–273, 1989.

[30] I. S. Adams, P. Gaiser, and W. L. Jones, "Simulation of the stokes vector in inhomogeneous precipitation," *Radio Sci.*, vol. 43, 2008, Art. no. RS5006, doi: 10.1029/2007RS003744.

[31] J. J. Coy, A. Bell, P. Yang, and D. L. Wu, "Sensitivity analyses for the retrievals of ice cloud properties from radiometric and polarimetric measurements in sub-mm/mm and infrared bands," *J. Geophys. Res. Atmos.*, vol. 125, 2020, Art. no. e2019JD031422, doi: 10.1029/2019JD031422.

[32] P. Eriksson et al., "A general database of hydrometeor single scattering properties at microwave and sub-millimeter wavelengths," *Earth Syst. Sci. Data*, vol. 10, pp. 1301–1326, 2018, doi: 10.5194/essd-10-1301-930 2018.

[33] I. Kaur, P. Eriksson, V. Barlakas, S. Pfreundschuh, and S. Fox, "Fast radiative transfer approximating ice hydrometeor orientation and its implication on IWP retrievals," *Remote Sens.*, vol. 14, 2022, Art. no. 1594, doi: 10.3390/rs14071594.

[34] P. Yang et al., "Spectrally consistent scattering, absorption, and polarization properties of atmospheric ice crystals at wavelengths from 0.2 to 100 μm," *J. Atmos. Sci.*, vol. 70, pp. 330–347, 2013, doi: 10.1175/JAS-D-12-039.1.

[35] C. M. Cooke et al., "A 220-GHz InP HEMT direct detection polarimeter," *IEEE Trans. Microw. Theory Techn.*, vol. 67, no. 12, pp. 5191–5201, Dec. 2019, doi: 10.1109/TMTT.2019.2944908.

[36] C. M. Cooke et al., "A 670 GHz integrated InP HEMT direct-detection receiver for the tropospheric water and cloud ice instrument," *IEEE Trans. THz Sci. Technol.*, vol. 11, no. 5, pp. 566–576, Sep. 2021, doi: 10.1109/TTHZ.2021.3083939.

[37] C. M. Cooke et al., "A 680 GHz direct detection dual-channel polarimetric receiver," in *Proc. IEEE/MTT-S Int. Microw. Symp.*, 2020, pp. 635–638, doi: 10.1109/IMS30576.2020.9224036.

[38] K. A. Shanks et al., "High-altitude demonstration of LWIR polarimetry using uncooled microbolometers," *J. Quantitative Spectrosc. Radiative Transfer*, vol. 315, 2024, Art. no. 108872, doi: 10.1016/j.jqsrt.2023.108872.

[39] S. C. Reising et al., "An earth venture in-space technology demonstration mission for temporal experiment for storms and tropical systems (tempest)," in *Proc. IEEE Int. Geosci. Remote Sens. Symp.*, 2018, pp. 6301–6303, doi: 10.1109/IGARSS.2018.8517330.

[40] S. C. Reising et al., "Tropospheric water and cloud ICE (TWICE) millimeter and submillimeter-wave radiometer instrument for 6U-class nanosatellites," in *Proc. 41st Int. Conf. Infrared, Millimeter, THz Waves*, 2016, pp. 1–2, doi: 10.1109/IRMMW-THz.2016.7758396.

[41] M. Ogut et al., "A novel 1/f noise mitigation technique applied to a 670 GHz receiver," *IEEE Trans. THz Sci. Technol.*, vol. 11, no. 1, pp. 109–112, Jan. 2021, doi: 10.1109/TTHZ.2020.3036179.

[42] P. Eriksson et al., "Towards an operational ice cloud imager (ICI) retrieval product," *Atmos. Meas. Techn.*, vol. 13, pp. 53–71, 2020, doi: 10.5194/amt-13-53-2020.

[43] D. L. Wu et al., "Chapter 10: IceCube: Submm-wave technology development for future science on a CubeSat," in *Proc. SPIE*, 2023, Art. no. PM347, doi: 10.1117/3.2618157.ch10.

[44] J. Gong, D. L Wu, and P. Eriksson, "The first global 883 GHz cloud ice survey: IceCube level 1 data calibration, processing and analysis," *Earth Syst. Sci. Data*, vol. 13, pp. 5369–5387, 2021, doi: 10.5194/essd-13-5369-2021.

DONG L. WU received the B.S. degree in space physics from the University of Science and Technology of China, Hefei, China, in 1985, the M.S. and Ph.D. degrees in atmospheric science from the University of Michigan, Ann Arbor, MI, USA, in 1993 and 1994, respectively. He was a Principal Research Scientist and the Supervisor of Aerosol and Cloud Group with Jet Propulsion Laboratory (JPL) with the California Institute of Technology, Pasadena, CA, USA, during 1994-2011. He was the Principal Investigator (PI) of Goddard's Ice-Cube project CubeSat flight demonstration of 883-GHz radiometer for cloud ice measurements. He was a Co-investigator with Microwave Limb Sounder (MLS) during 1994-2008, CloudSat during 2006-2010, Multi-angle Imaging SpectroRadiometer (MISR) since 2008, and NASA's Global Navigation Satellite Systems (GNSS) since 2007. He is currently the Project Scientist of NASA's Total and Spectral Solar Irradiance Sensor (TSIS) mission with Goddard Space Flight Center (GSFC). He authored or coauthored more than 180 papers on peer-reviewed journals. His research interests include remote sensing of atmospheric clouds and winds, and ionospheric electron density. He was the recipient of several awards, including NASA Exceptional Achievement Medal in 2001, 2008 and 2022, JPL Ed Stone award for Outstanding Research Paper in 2006, and Robert H. Goddard Award for Science in 2019.

JIE GONG (Member, IEEE) received the Ph.D. degree from Stony Brook University, Stony Brook, NY, USA and undergraduate training from Peking University, Beijing, China. She joined NASA Goddard Space Flight Center (GSFC) Climate and Radiation Lab in 2022. Her research interests span across multitudes, from ice cloud/frozen hydrometeor remote sensing to atmospheric gravity waves, from boundary layer water vapor to lower atmosphere - ionosphere/thermosphere coupling. Her current projects focus on developing better frozen hydrometeor retrieval algorithms for next generation radiometers, expanding machine learning techniques to better solve atmospheric science problems, understanding lower-upper atmosphere coupling using satellite observations, model simulations, and ML techniques.

WILLIAM R. DEAL (Fellow, IEEE) received the B. S. degree in electrical engineering from the University of Virginia, Charlottesville, VA, USA, in 1996, the M.S. and Ph.D. degrees from the University of California, Los Angeles, CA, USA, in 1998 and 2000, respectively. He is currently a Consulting Engineer with Northrop Grumman's RF Product and Mixed Signal Center, Redondo Beach, CA, USA. He leads a variety of efforts related to developing submillimeter wave technology and inserting submillimeter wave technology into applications. He has authored or coauthored more than 150 journal and conference papers, as well as five book chapters. He was recipient of the Outstanding Young Engineer Award in 2009, 2012 IEEE "Tatsuo Itoh" Best Microwave and Component Letter Paper, and 2016 IEEE Electron Device Letters "George E. Smith" Best Paper Award.

WILLIAN GAINES (Member, IEEE) received the B.S. degree in mechanical engineering from California State University at Long Beach in 1981. He is currently a Technical Fellow with Northrop Grumman. He is also the Supervisor for the Engineering Development Lab, the Azusa campus. As a packaging SME, he supports various programs in Azusa, providing expertise in board design, cable & harness design and EMI & RFI solutions. As part of the Aerojet heritage at Azusa, he was the principal packaging engineer for SSMIS during 1988–1995 and AMSU-EOS/METSAT during 1995–1998 instruments. He was with Ford Aerospace, Newport Beach during 1981–1987. He is a past president of the Orange Chapter of IMAPS during 1995–2018

CAITLYN M. COOKE (Member, IEEE) received the B.S. and M.S. degrees in electrical engineering in 2014 and 2016, respectively from the University of Colorado, Boulder, CO, USA, where she is currently working toward the Ph.D. degree in electrical engineering. From 2014 to 2017, she was with NASA Goddard Space Flight Center, Greenbelt, MD, USA, involved with submillimeter-wave radiometers for CubeSats. She received the NASA Space Technology Research Fellowship in 2016, for research on millimeter-wave monolithic microwave integrated circuits for radiometer front-ends. She is currently an RF Design Engineer with Northrop Grumman Aerospace Systems, Redondo Beach, CA, USA, where she is focused on high frequency MMIC design and packaging.

GIOVANNI DE AMICI received the Laurea degree in physics from the University' degli Studi of Milano, Milano, Italy, in 1978, and the Dottorato di Ricerca degree in astronomy from the Ministero Pubblica Istruzione of Roma, Rome, Italy, in 1986. He was a Research Associate with the Space Science Laboratory, University of California, Berkeley, Berkeley, CA, USA, and a Staff Member with TRW and Northrop-Grumman. He is currently the Engineering Directorate with NASA's Goddard Space Flight Center, Greenbelt, MD, USA. His research interests focus on technologies for remote sensing of the environment, from the surface of last scattering in cosmology to weather and climate on Earth.

PETER PANTINA received the M.S. degree in meteorology from Florida State University, Tallahassee, FL, USA, in 2011. He joined Science Systems and Applications, Inc. as a contractor with NASA Goddard Space Flight Center in 2011. Since then, he has provided instrument and systems engineering support for ~20 ground-based, airborne, and space-flight Earth science field campaigns.

YULI LIU received the B.S. degree from Xidian University, Xi'an, China, in 2012, and the Ph.D. degree from the University of Chinese Academy of Sciences, Beijing, China, in 2018. From 2016 to 2018, he was a visiting Ph.D. student with the University of Hamburg, Hamburg, Germany, supervised by Professor Stefan Buehler. He was a Postdoctoral Research Associate with the University of Utah, Salt Lake City, UT, USA, under the guidance of Professor Gerald G. Mace from 2018 to 2022. Since 2022, he has been an Assistant Research Scientist with the Goddard Earth Sciences Technology and Research (GESTAR) II, University of Maryland, Baltimore County. His research focuses on ice cloud remote sensing using (sub)millimeter-wave radiometer and microwave radar.

PING YANG received the B.S. degree in theoretical physics from Lanzhou University, Lanzhou, China, in 1985, the M.S. degree in atmospheric physics from the Lanzhou Institute of Plateau Atmospheric Physics, Chinese Academy of Sciences, Lanzhou, in 1988, and the Ph.D. degree in meteorology from The University of Utah, Salt Lake City, USA, in 1995. He was with The University of Utah for two years as a Research Associate. He was an Assistant Research Scientist with the University of California, Los Angeles, CA, USA, and an Associate Research Scientist with the Goddard Earth Sciences and Technologies Center, University of Maryland Baltimore County, Baltimore. He has been actively conducting research in the modeling of the optical and radiative properties of clouds and aerosols, particularly cirrus clouds, and their applications to spaceborne and ground-based remote sensing. He is a member of the MODIS Science Team. He is currently a Professor and the holder of the David Bullock Harris Chair in Geosciences with the Department of Atmospheric Sciences, Texas A&M University, College Station, TX, USA. He has coauthored more than 160 peer-reviewed publications. His research interests include remote sensing and radiative transfer. He is currently an Associate Editor for *Journal of Atmospheric Sciences*, *Journal of Quantitative Spectroscopy and Radiative Transfer*, and *Journal of Applied Meteorology and Climatology* and is also on the Editorial Board for *Theoretical and Applied Climatology*. He was the recipient of the Best Paper Award from the Climate and Radiation Branch, National Aeronautics and Space Administration Goddard Space Center, in 2000, U.S. National Science Foundation CAREER Grant in 2003, and Dean's Distinguished Achievement Award for Faculty Research, College of Geosciences, Texas A&M University, in 2004. He is a fellow of the Optical Society of America.

PATRICK ERIKSSON received the graduation degree in engineering physics and the Ph.D. degree in environmental sciences from Chalmers University of Technology, Gothenburg, Sweden, in 1990 and 1999, respectively. He is currently a Professor of global environmental measurements with Chalmers University of Technology. His main areas of expertise are atmospheric radiative transfer and retrieval methodologies, with a focus on passive microwave sounding of the atmosphere. He is an ECMWF Fellow in the area of radiative transfer. He is a core member of the team working on the submillimeter radiometer on board the Odin satellite and a member of the science advisory group for the upcoming EUMETSAT MicroWave Imager and Ice Cloud Imager missions. With Stefan Buehler (University of Hamburg), he is leading the development of the Atmospheric Radiative Transfer System (ARTS) open-source software. He implemented the Qpack inversion package complementing ARTS and has extensive experience in using machine learning to retrieve data from satellite observations. He has authored or coauthored about 135 peer-reviewed journal articles.

RALF BENNARTZ received the M.S. degree in atmospheric physics from the University of Hamburg, Hamburg, Germany, in 1994 and the Ph.D. degree from the Free University of Berlin, Berlin, Germany, in 1997. Since 2002, he has been with the faculty of the Atmospheric and Oceanic Sciences Department, University of Wisconsin-Madison and Principal Investigator with the University of Wisconsin's Space Science and Engineering Center. His research interests include satellite remote sensing and atmospheric radiative transfer in the near-infrared and microwave spectral range., He was also a Past Editor during 2006–2010 of the American Meteorological Society's *Journal of Applied Meteorology and Climatology*.